

Four-month chromospheric and coronal activity cycle in τ Boötis

M. Mittag¹, J. Robrade¹, J. H. M. M. Schmitt¹, A. Hempelmann¹, J. N. González-Pérez¹, and K.-P. Schröder²

¹ Hamburger Sternwarte, Universität Hamburg, Gojenbergsweg 112, 21029 Hamburg, Germany
e-mail: mmittag@hs.uni-hamburg.de

² Department of Astronomy, University of Guanajuato, 36000 Guanajuato, Mexico

Received 21 June 2016 / Accepted 13 January 2017

ABSTRACT

We have used our robotic TIGRE facility to closely monitor the star τ Boo during the last three observing seasons 2013–2016 and to determine its S -index variability from the strength of its Ca II H and K line cores in order to study its characteristic cyclic chromospheric variations and determine its rotation period. We furthermore reanalyze archival X-ray data of τ Boo taken with the *XMM-Newton* satellite. Using Lomb-Scargle periodograms, we find a strong periodic signal in our data with a period of about 122 days with extremely high significance, which is also consistent with the observed long-term X-ray variability. Furthermore, the epochs of magnetic field reversals observed in τ Boo with the technique of Zeeman Doppler imaging are consistent with the hypothesis that they are produced at activity maximum. In line with previous studies of τ Boo, we therefore interpret our data as evidence of a very short activity cycle in analogy to the solar cycle, but the cycle period of τ Boo may also show some slight variability and may show substantial phase shifts. The chromospheric signal of τ Boo is found to vary on the rotational timescale of somewhat more than three days only during one out of the available three observing seasons. The available data suggest that persistent cyclic magnetic activity can occur on timescales much shorter than the decadal timescale observed for the Sun and many other late-type stars.

Key words. stars: activity – stars: chromospheres – stars: late-type – stars: individual: τ Boo

1. Introduction

The physics underlying the 22-yr solar magnetic activity cycle is still not well understood, and the same applies to stellar activity cycles. An important if not the most important technique to diagnose stellar activity cycles is the study of the emissions in the Ca II H and K line cores, which seems to have first been recognized by Eberhard & Schwarzschild (1913). In the Sun (and in solar-like stars) this core emission is caused by bright chromospheric “plage” regions that systematically vary over the solar cycle, and in particular allow a study of the solar cycle in disk-integrated, that is, stellar-like light by suitable long-term monitoring campaigns. As shown by Wilson (1978), Baliunas et al. (1995), Hall et al. (2007), Isaacson & Fischer (2010), and Hempelmann et al. (2016), such monitoring data can be used to infer both stellar rotation and stellar activity cycles. Baliunas et al. (1995) presented several decades of data for 112 stars from the Mount Wilson project and determined activity cycles for more than 40 stars, with the typical cycle periods varying from 2.5 yr to more than 20 yr.

Baliunas et al. (1995) specifically presented the S -index time series of τ Boo (=HD 120136), which shows a chromospheric cycle of 11.6 ± 0.5 yr. τ Boo is a bright ($m_V = 4.5$ mag) star of spectral type F7 with an M2 type companion, which was observed several thousand times during the Mount Wilson program. Today, there is great interest in τ Boo as a planet-hosting star (Butler et al. 1997). The period of the hot Jupiter orbiting around τ Boo is 3.3 days, very close to the presumed rotation period of τ Boo; if the two periods were identical, τ Boo and τ Boo b would be synchronized.

However, there is some uncertainty concerning the rotation period of τ Boo. Catala et al. (2007) summarized this

very precisely. These authors pointed out that the rotation period of τ Boo is not well known and is between 2.6 and 4.1 days (Henry et al. 2000). Furthermore, they mentioned the hypotheses from different authors (Leigh et al. 2003; Collier Cameron & Leigh 2004; Shkolnik et al. 2005) that the star and the planet are tidally locked and so the rotation period of the star would be 3.31 days. However, Catala et al. (2007) also pointed out that this has never been observed directly. This statement made by Catala et al. in 2007 still appears to be true. A relevant piece of information on the rotation period of τ Boo comes from the MOST satellite, which observed τ Boo on two occasions: for 11.5 days in 2004, and for 21.6 days in 2005. Walker et al. (2008) presented a detailed analysis of these data and found a period of 3.5 ± 0.7 days in the 2004 data, but no signal in the 2005 data. Based on their analysis, Walker et al. (2008) concluded that this period might be induced by the synchronized planet and not by spots. In the context of their Doppler imaging, Donati et al. (2008), Fares et al. (2009, 2013) and Mengel et al. (2016) determined rotation periods (given in units of Ω_{eq} in rad d^{-1} : 2.10 ± 0.04 , 1.86 ± 0.02 , 1.93 ± 0.02 , 2.05 ± 0.04 , 2.12 ± 0.12 , 1.98 ± 0.01 , 2.03 ± 0.05 , 2.05 ± 0.04 , 1.95 ± 0.01 , 1.99 ± 0.01 , and 1.98 ± 0.03) and the strength of differential rotation ($d\Omega$ in rad d^{-1} : 0.50 ± 0.12 , -0.18 ± 0.07 , 0.28 ± 0.10 , 0.42 ± 0.10 , 0.50 ± 0.15 , 0.15 ± 0.03 , 0.42 ± 0.11 , $0.38^{+0.18}_{-0.19}$, 0.16 ± 0.04 , 0.10 ± 0.04 , and $0.15^{+0.15}_{-0.16}$). We refer to the individual papers for a detailed discussion of these values, while Reiners (2006) determined the strength of the differential rotation ($d\Omega = 0.31 \pm 0.134 \text{ rad d}^{-1}$) of τ Boo using line profile modeling. From these given values, we obtain an averaged period of 3.1 days with a standard deviation of 0.1 days, and for the differential rotation without the negative value, we derive an averaged $d\Omega$ of 0.31 rad d^{-1} with a standard deviation of 0.15 rad d^{-1} . At

this point, we note that because of the differential rotation, we can expect a larger scatter of the rotational period measured in different epochs.

X-ray and hence coronal emission from τ Boo was first detected with the *Einstein* Observatory at $\log L_X = 28.9 \text{ erg s}^{-1}$ (Schmitt et al. 1985) and later by ROSAT (Hünsch et al. 1998). Several dedicated X-ray observations by *XMM-Newton* and *Chandra* were carried out over the past several years: Maggio et al. (2011) presented an analysis of the deep *XMM-Newton* observation taken in 2003, and Poppenhaeger et al. (2012) and Poppenhaeger & Wolk (2014) studied and characterized the X-ray emission of the τ Boo system in greater detail.

In addition to the 11.6 yr cycle, there is evidence of cyclic variability on substantially shorter timescales. Baliunas et al. (1997) described an additional variation of 116 days in their S_{MWO} time series without providing any details of this variation, however. τ Boo was also monitored in the context of different projects and different instruments, for example, at the Lowell Observatory (Hall et al. 2007), the CPS program (Isaacson & Fischer 2010), and with the NARVAL instrument (Mengel et al. 2016). Specifically, Mengel et al. (2016) deduced a 117-day period in their S -index time series taken with the NARVAL instrument, which they identified with the 116-day period reported by Baliunas et al. (1997) and Henry et al. (2000). Furthermore, based on spectropolarimetric observations with ESPaDOnS and NARVAL and using the Zeeman Doppler imaging (ZDI) technique, Donati et al. (2008) provided evidence of a magnetic polarity reversal, and the analysis of Fares et al. (2013) of several such field reversals suggested a possible magnetic cycle of 240 or 740 days, which would then point at a chromospheric cycle period of 120 or 370 days; further field reversals have been reported by Mengel et al. (2016). Short cycles with periods below one year appear somewhat unusual, but we note that Metcalfe et al. (2010) reported a very short activity cycle of 1.6 yr for the F8 star ι Hor. Furthermore, García et al. (2010) reported that they found an indication of a cycle with a period of at least 120 days for HD 49933.

In this paper we present S -index monitoring observations of τ Boo during the three observing seasons 2013–2016 and a re-analysis of all archival X-ray data to ensure consistent analysis procedures. With these results and the published ZDI maps from Fares et al. (2013) and Mengel et al. (2016), we investigate connections between the different magnetic activity indicators and study the cyclic behavior of τ Boo as well as its variations over the past years.

2. Observation and data reduction

2.1. TIGRE data

We carried out intensive activity monitoring of τ Boo using our TIGRE facility located at the La Luz Observatory near Guanajuato, Mexico. TIGRE is a 1.2 m fully robotic telescope, its main instrument being the two-arm fiber-fed Échelle spectrograph HEROS with a spectral range from $\approx 3800 \text{ \AA}$ to 8800 \AA with a small gap at 5800 \AA and a spectral resolution $R \approx 20\,000$; a detailed description of the TIGRE facility is given by Schmitt et al. (2014).

As part of our stellar activity monitoring program at Hamburg and Guanajuato, τ Boo was regularly observed in the observing seasons 2013–14, 2014–15, and 2015–16; we often achieved a nightly observing cadence necessary to study the short rotational period of about three days. The individual exposure times were adapted for each observation to achieve a

Table 1. TIGRE observational data.

Season	First date	Last date	No. of S_{MWO}	S/N
2013/14	2013-12-18	2014-08-14	77	65
2014/15	2014-12-24	2015-06-11	73	78
2015/16	2016-01-08	2016-05-09	88	76

Notes. Observational season, start, and end (YY-MM-DD) of time series, number of used S -indices, and the mean S/N in the Ca II H and K region ($3880\text{--}4020 \text{ \AA}$)

specified signal-to-noise ratio (S/N) at a given wavelength. Thus, the S/N in the Ca II H and K region should approximately have the same level, and here we use only data with a S/N higher than 40 in the Ca II H and K region. In Table 1 we list the time range of each time series, the number of the S -indices, and the mean S/N in the Ca II H and K region from 3880 \AA to 4020 \AA . For our analysis we use 238 spectra taken between December 2013 and May 2016.

The recorded spectra are reduced with the fully automatic standard reduction pipeline for the TIGRE/HEROS spectra. This pipeline is implemented in IDL and based on the reduction package REDUCE (Piskunov & Valenti 2002). The TIGRE/HEROS standard reduction pipeline performs all necessary reduction steps to reduce Échelle spectra: bias subtraction, order definition, wavelength calibration, spectra extraction, and flat fielding. Additional information can be found in Hempelmann et al. (2016) and Mittag et al. (2016).

As a part of the TIGRE/HEROS reduction pipeline, the instrumental S -index of the Ca II H and K lines (thereafter, S_{TIGRE}) is computed. This index is defined as

$$S_{\text{TIGRE}} = \left(\frac{N_{\text{H}} + N_{\text{K}}}{N_{\text{R}} + N_{\text{V}}} \right), \quad (1)$$

where N_{H} and N_{K} are the integrals of the Ca II H and K line intensities in a rectangular bandpass of 1 \AA at the line centers, and N_{R} and N_{V} the integrals of two 20 \AA wide bandpasses centered on 3901.07 \AA and 4001.07 \AA . This instrumental S -index is converted into the commonly used activity index, the so-called Mount Wilson S -index (thereafter, S_{MWO}), using the transformation equation

$$S_{\text{MWO}} = 0.0360 + 20.02S_{\text{TIGRE}}. \quad (2)$$

Mittag et al. (2016) describe the computation of the S_{TIGRE} and the transformation of the S_{TIGRE} into S_{MWO} in detail.

2.2. X-ray data

The τ Boo system was observed with the *XMM-Newton* satellite on a number of occasions. The observations used are summarized in Table 2, the data taken between July 2011 and January 2012, that is, three observations, are presented here for the first time. All observations were performed with the thick filter and thus provide a rather homogeneous dataset. A detailed description of the instruments and software can be found in the *XMM-Newton* Users Handbook and the SAS Users Guide¹. The X-ray data were rereduced, and the analysis was carried out with the *XMM-Newton* Science Analysis System (SAS) version 13.5 (de la Calle 2014). Standard SAS tools and selection criteria were used to produce images, light curves, and spectra.

¹ <http://www.cosmos.esa.int/web/xmm-newton>

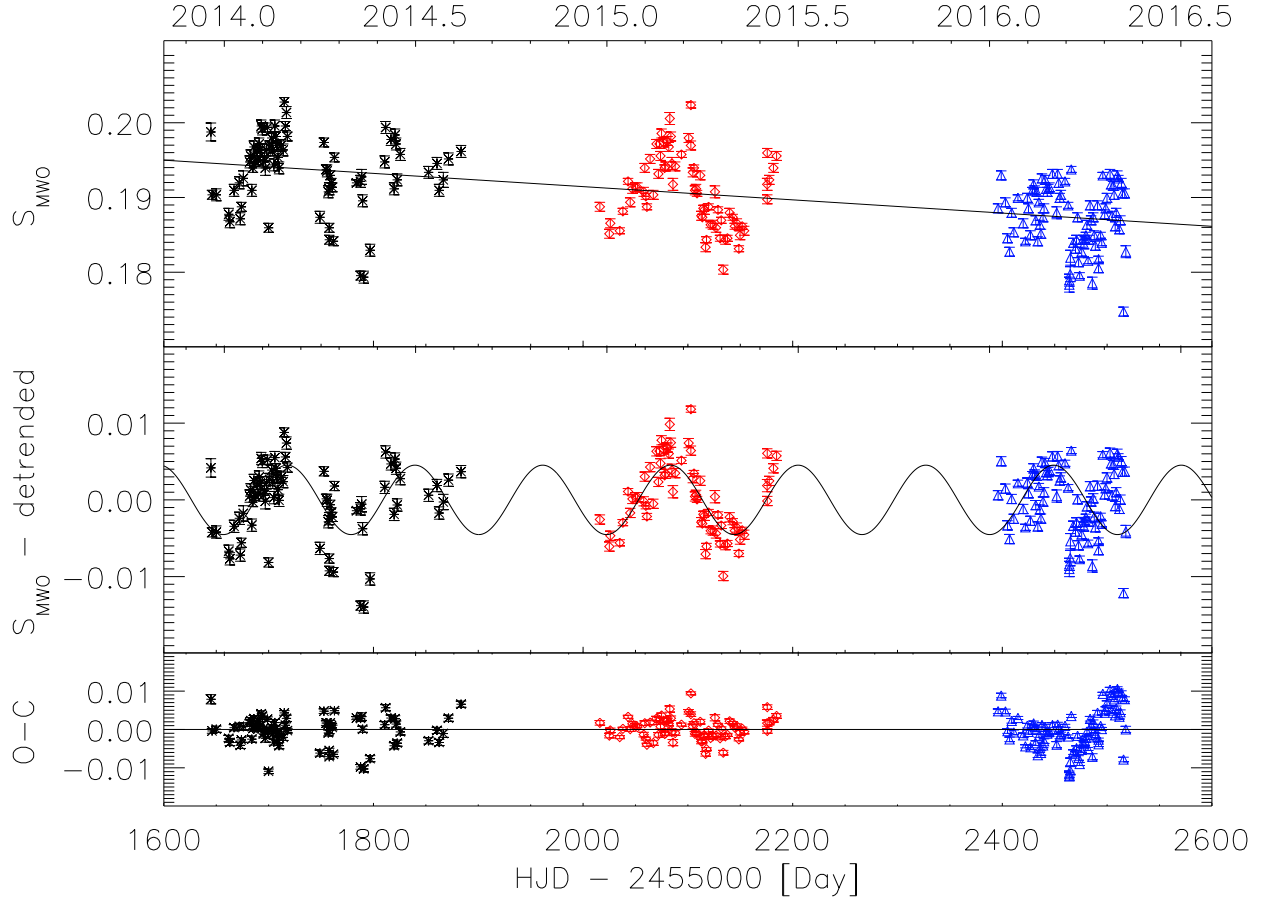


Fig. 1. TIGRE S_{MWO} time series of τ Boo. The three observation seasons are color coded: black for 2013–14, red for 2014–15, and blue for 2015–16. *Upper panel:* raw time series with the solid line representing the polynomial fit used for the detrending. *Middle panel:* detrended time series with the sinusoidal fit. *Bottom panel:* fit residuals (O–C). The different symbols and colors represent the different observation seasons.

Table 2. *XMM-Newton* observing log.

Date	MJD_start	Obs. ID	Dur. (ks)
2003-06-24	52 814.1	0144570101	64
2010-06-19	55 366.4	0651140201	13
2010-07-23	55 400.3	0651140301	8
2010-12-20	55 550.0	0651140401	8
2011-01-23	55 584.0	0651140501	11
2011-06-19	55 731.5	0671150501	10
2011-07-15	55 757.5	0671150601	10
2011-12-24	55 919.0	0671150701	9
2012-01-20	55 946.8	0671150801	9

Since we are primarily interested in X-ray luminosities of τ Boo, we focused on data taken with the European Photon Imaging Camera (EPIC) detector, the most sensitive instrument onboard *XMM-Newton*. The spectra of each individual observation are fit with two-temperature APEC models (Smith et al. 2001) to derive the X-ray fluxes and coronal properties of τ Boo. These models use a calculated emission spectrum from a collisionally ionized diffuse gas calculated using the ATOMDB code and a coronal abundance pattern. The free parameters for each plasma component are its temperature and emission measure, with $EM = \int n_e n_H dV$.

The τ Boo binary (F7 + M2, sep. 2'') is unresolved in the *XMM-Newton* data, but two datasets of the resolved system are

available from *Chandra*. These data allow us to determine accurate photon flux ratios between the two components because of the superior angular resolution of the *Chandra* telescope. We find 475 counts for the A component and 150 for the B component in one observation (ID 13232, 5.0 ks) and 475 counts and 85 counts, respectively, in a second observation (ID 13233, 4.9 ks) in our analysis of the ACIS-I data, showing that the M dwarf typically contributes about 20% to the total X-ray flux. The derived system X-ray luminosities are consistent with the *XMM-Newton* values, but because of larger uncertainties, they are not included in the variability study. All results used for the study of possible cyclic activity are derived from *XMM-Newton* data given in the 0.2–3.0 keV energy range and are obtained from the sum of the components. Nevertheless, inspection of the spatial photon distributions and X-ray light curves indicates that the X-ray emission of the system is strongly dominated by the primary at all times.

3. Results

3.1. *S*-index: long-term variations

In Fig. 1 we plot our TIGRE S_{MWO} time series; in all three panels the black data points refer to data taken in the season 2013–14, the red data points plot data from the season 2014–15, and the blue data points show data from the season 2015–16. The observed mean value for our S_{MWO} time series is 0.190 ± 0.001 and agrees well with the mean S_{MWO} of

0.191 reported by [Baliunas et al. \(1995\)](#). We plot the raw S -index data in the upper panel of Fig. 1, the linearly detrended S -index data in the middle panel of Fig. 1, and the residuals S -index data in the lower panel of Fig. 1. The raw data show a clear periodic behavior, and a weak linear trend is visible. A trend in a time series can lead to changes in the periodogram power spectrum and to shifts in the obtained periods of maximal power. A possible trend must therefore be removed, but a possible trend is not considered in the common Lomb-Scargle approach presented by [Horne & Baliunas \(1986\)](#) or by [Zechmeister & Kürster \(2009\)](#). Both authors used an approach with pure sine waves, and [Zechmeister & Kürster \(2009\)](#) considered an additional constant offset. In our TIGRE data, we find only a linear trend, shown as solid line in Fig. 1, which may be ascribed to the 11.6 yr cycle reported by [Baliunas et al. \(1995\)](#) and which we removed before performing any Fourier analysis.

After detrending, we computed a Lomb-Scargle (LS) periodogram using the method by [Horne & Baliunas \(1986\)](#) to estimate the period of the visible variation. We estimate the period uncertainty using the equation (cf., [Baliunas et al. 1995](#))

$$\Delta P = \frac{3\sigma_n P^2}{4TA\sqrt{N}}, \quad (3)$$

where P is the period, σ_n the standard deviation of the residuals, T the total length of the observation interval, A the amplitude of the signal, and N the total number of data points. We compute a false-alarm probability (FAP) using the common expression (cf., [Horne & Baliunas 1986](#))

$$\text{FAP} = 1 - (1 - e^{-z})^{N_i}, \quad (4)$$

where z is the height of the corresponding peak in the periodogram and N_i is the number of independent frequencies. The critical and problematic part for the FAP estimation is the determination of the number of independent frequencies. One method to estimate the FAP without exact knowledge of the number of independent frequencies is the bootstrapping method (e.g., [Cumming et al. 1999](#)). However, this method is very time consuming and unpractical, especially when the main peak is very high and the time span is very long, as in our case. A more practical and quick method to estimate the FAP is described by [Zechmeister & Kürster \(2009\)](#), who estimated the number of independent frequencies from the widest possible frequency range and the frequency resolution. They reported an elegant and practical way to estimate the number of independent frequencies and hence the FAP. Therefore, we used the method described by [Zechmeister & Kürster \(2009\)](#) for our estimation of the number of independent frequencies and for all our FAP estimations.

To determine the period of the time series, we only used data until day 2463 [HJD-2 455 000] (2013–16 until 2463 [HJD-2 455 000]), since after this date a very pronounced change occurs in the time series of S values (see below). Maximal power is found for a period of 121.8 ± 0.7 days with a formal FAP of 9.3×10^{-17} , corresponding to a formal significance of more than 7σ . The window function is shown in Fig. 3. In Fig. 2 we plot the derived LS periodogram (dotted line) together with the FAP at 7σ ; in Fig. 4 we show the phase-folded time series with the same color symbols as in Fig. 1. Additionally, we determine the period for the total time series obtained between 2013 and 2016 to show the influence of the jump at day 2463 [HJD-2 455 000] on the period. Furthermore, we determine the period considering only data obtained in the first two seasons (i.e., in 2013–14 and 2014–15) and list the results in Table 3.

We identify “our” cycle period of ≈ 122 days and note that this value is comparable with the 116-day period reported

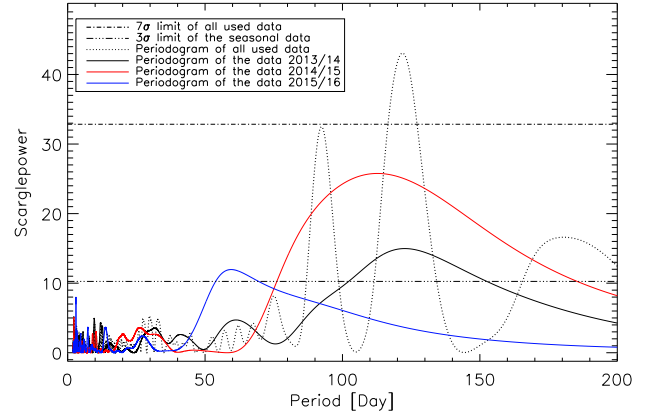


Fig. 2. Periodograms of the TIGRE τ Boo time series; the dotted line shows the periodogram of the LS analysis for the data until 2463 [HJD-2 455 000], the solid and color-coded lines show the periodograms of the LS analysis for the seasonal data with the coding scheme as used in Fig. 1. Furthermore, the formal 7σ limit for the data until 2463 [HJD-2 455 000] is shown as a dash-dotted line and the mean 3σ limit of the seasonal data as a dash-triple-dotted line.

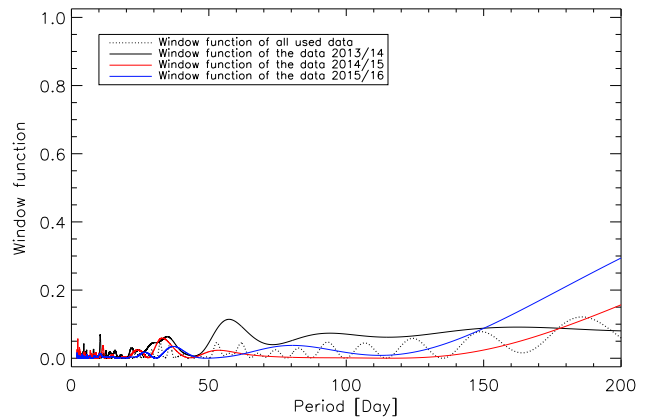


Fig. 3. Window functions of the TIGRE τ Boo time series; the dotted line shows the window function for the data until 2463 [HJD-2 455 000], the solid and color-coded lines show the window function for the seasonal data with the coding scheme used in Fig. 1.

by [Baliunas et al. \(1997\)](#) and the 117-day period reported by [Mengel et al. \(2016\)](#). The 122-day period is shown as a solid line in the middle plot of Fig. 1, and the lower plot shows the residuals of this sinusoidal fit. The residuals are not randomly distributed, rather they show trends, in particular for the observing season 2015–16. This indicates that the global fit with a period of 121.8 days does not provide a perfect fit and that the length and amplitude of the cycle may possibly change; these phenomena are well known for the solar cycle, especially for the sunspot number (e.g., [Oláh et al. 2016](#), see Fig. 1).

In order to test how our assumption of a linear trend affects the derived period, we estimated the trends using polynomials of different order and derived the periods as described above after the trend removal; these results are listed in Table 4. Inspection of Table 4 shows that the peak power indeed increases when the time series is detrended. However, polynomials of order two or higher do not provide any significant increase compared to a linear trend, and thus we conclude that the usage of a linear trend is adequate. Additionally, we detrended the data by subtracting the seasonal mean from the corresponding seasonal

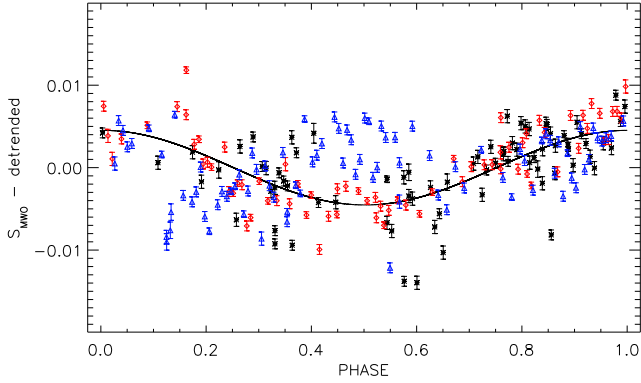


Fig. 4. Phase-folded S_{MWO} time series of τ Boo; the color code is the same as in Fig. 1.

Table 3. Cycle period of different time spans, period FAP, and the cycle amplitude.

Season	Period [Day]	FAP
2013–16 until 2463 [HJD-2 455 000]	121.8 ± 0.7	9.3×10^{-17}
2013–15	120.5 ± 1.0	1.6×10^{-15}
2013–16	117.4 ± 0.8	9.4×10^{-14}

Table 4. Results of detrending tests.

Detrending with	Period	Peak height
No detrending	127.8 ± 0.9	38.5
Polynomial fit of first order	121.8 ± 0.7	43.1
Polynomial fit of second order	122.0 ± 0.7	43.5
Polynomial fit of third order	122.0 ± 0.7	43.5
Detrending with the seasonal mean	121.8 ± 0.7	43.6
Polynomial fit of first order (slope $+1\sigma$)	122.4 ± 0.7	42.2
Polynomial fit of first order (slope -1σ)	121.3 ± 0.7	43.9

data and obtained the same results as with linear detrending. Finally, we tested the influence of the trend uncertainty on the estimated periods. We added and subtracted, respectively, the 1σ error of the slope from the estimated slope, detrended the time series with these new slopes, and estimated the new period (see Table 4 for a polynomial fit of first order (slope $+1\sigma$) and (slope -1σ)). All test results are listed in Table 4. We conclude that our conclusions do not depend on the details of the trend removal as long as some detrending is performed.

3.2. S -index: seasonal variations

We now proceed by analyzing the individual observing seasons separately, since the S -index time series obtained in each observation season are long enough to allow a period estimate in each single observation season. The results of these period estimates are listed in Table 5, and the corresponding periodograms are also shown in Fig. 2 with the the same color code as used in Fig. 1. Furthermore, the window functions for each single observation season are shown in Fig. 3. Inspection of Table 5 shows that the periods derived in the seasons 2013–14 and 2014–15 are more or less comparable, while we find a period of only ≈ 60 days

Table 5. Seasonal cycle period, period FAP, the cycle amplitude, and estimated date of cycle maximum.

Season	Period [Day]	FAP	Amplitude [detrended S_{MWO}]	Cycle max HJD – 2 455 000 [Day]
2013–14	122.7 ± 4.2	3.0×10^{-5}	0.0048	1718.0
2014–15	112.7 ± 3.0	6.0×10^{-10}	0.0055	2083.5
2015–16	59.5 ± 2.8	3.2×10^{-4}	0.0030	2447.9

Notes. The error of the estimated amplitude is ≈ 0.0001 for all three seasons.

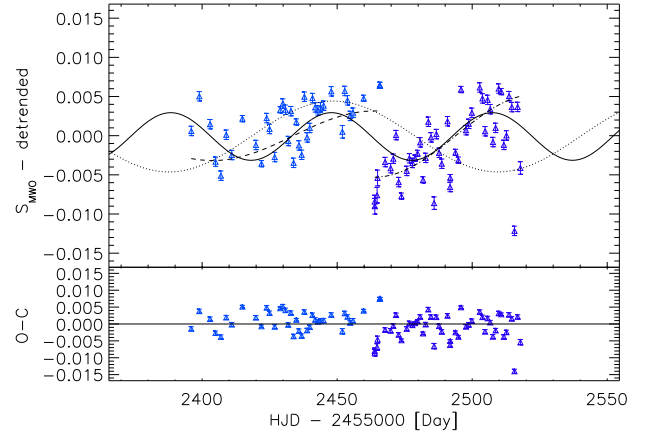


Fig. 5. Detrended S_{MWO} time series of the observing season 2015–16. *Upper panel:* sinusoidal fit with a the period of 59.5 days (solid curve); best fit with a 121.8-day cycle estimated from the data until 2463 [HJD-2 455 000] (dotted curve); ad hoc fit with a sine curve of 120.5 days with adapted amplitude and phase as well as phase shift (dashed and dash-dotted curve). See text for details. *Lower panel:* residuals of the sinusoidal fit with the period of 59.5 days.

in the season 2015–16. In Fig. 5 a zoom-in of the data taken in season 2015–16 is shown. The solid line indicates a sinusoidal fit with a period of ≈ 60 days.

A closer inspection of the S -index data taken in season 2015–16 (cf., Fig. 5) demonstrates that this cycle behaves differently. At the beginning of the TIGRE observations in early 2016, the cycle starts normally with increasing S_{MWO} index values, as expected from the 122-day period. However, at or near the cycle maximum, the S_{MWO} -index values suddenly, that is, within a week or so, jump to minimum values, and afterward, the S_{MWO} indices again start to increase. The S -index light curve looks as if the cycle had been stopped at or close to maximum and then restarted at zero, which explains why the LS periodogram for the observation season 2015–16 peaks at half the expected period.

To demonstrate this behavior more quantitatively, we zoom in on the data obtained during this last observing season in Fig. 5. The formally best fit with a cycle period of ≈ 60 days is shown by the solid line, while the best fit to all data until day 2463 [HJD-2 455 000] with a 121.8-day period is shown by the dotted curve. Clearly, this latter curve provides a good description for the data before day 2463, but a very poor description for the data taken thereafter. When we instead consider only the rising part of a cycle with a period of ≈ 121 days obtained from the two first cycles (season 2013–15, see Table 3) and an adapted amplitude and phase (plotted as a dashed curve in Fig. 5), and phase shift this curve ad hoc by half a cycle at day 2463 for the data taken thereafter (plotted as a dash-dotted curve in Fig. 5),

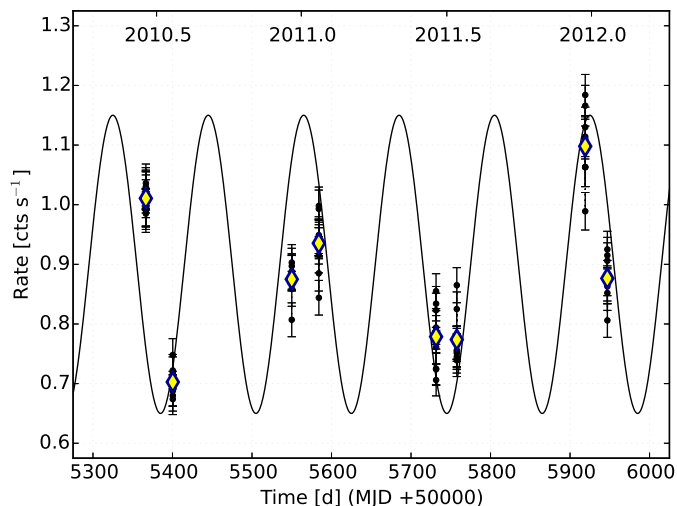


Fig. 6. X-ray light curve from EPIC pn data with 1 ks binning (black dots) and observational means (diamonds). A cycle model is overplotted.

we obtain a decent description of our TIGRE data. To quantify how well these periods fit the data of the season 2015–16, we calculated the standard deviation of the corresponding residuals and found a standard deviation of 0.0036 for the ≈ 60 -day period, a standard deviation of 0.0052 for the ≈ 122 -day period, and a standard deviation of 0.0036 when only the rising part of the 120-day cycle is considered. Thus, a sinusoidal fit of ≈ 60 days and the model considering only the rising part of a ≈ 121 cycle fit equally well.

The question is whether this type of jump could be of instrumental nature. However, the instrumental setup was not changed during the measurements, and no such jumps are observed in the time series of other stars. We therefore exclude an instrumental nature of the S -index jump observed for τ Boo during the season 2015–16.

3.3. X-ray emission

The X-ray light curve of τ Boo obtained from the available *XMM-Newton* observations is plotted in Fig. 6 and shows brightness variations on timescales of several months. The sparse X-ray data make an independent period analysis not very meaningful. We instead overplot a sinusoidal variation with period and activity maxima taken from spectropolarimetric and chromospheric measurements (Fares et al. 2013; Mengel et al. 2016). These data overlap in time with the X-ray campaign performed in 2010–2012. We adopted a period of 120 days, which is half of the magnetic cycle period given in Fares et al. (2013) for the signed magnetic flux; the uncertainties in period and phase are on the order of a few days. Furthermore, the near-simultaneous measurements from Fares et al. (2013) and Mengel et al. (2016) allow us to study possible connections between the X-ray emission, Ca II H and K, and magnetic polarity reversals.

We consider the match between X-ray brightness and cyclic model to be reasonable overall, especially given the presence of a companion, intrinsic short-term variability, and possible variations in amplitude and length of the cycle. The individual exposures exhibit short-term variability at a level of up to about 10% and some minor activity. The origin of this short-term variability cannot be unambiguously assigned to one of the components, but our results are clearly not affected by any strong flares.

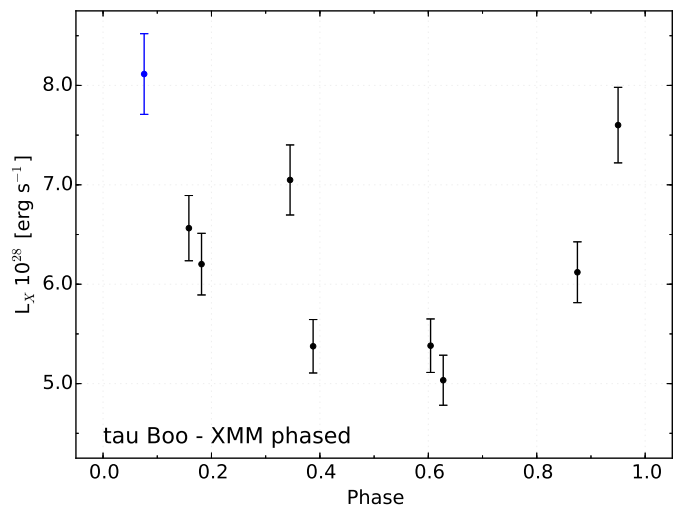


Fig. 7. Phase-folded X-ray luminosity of τ Boo ($P_{\text{cyc}} = 120$ d). The data for 2010–2012 (black) and 2003 (blue) are shown.

The comparison of the three magnetic activity indicators shows that they basically follow the same underlying cyclic pattern. The period of the coronal cycle is identical to the chromospheric period and half of the period determined for the magnetic field cycle (polarity reversal), although X-ray emission is not sensitive to the sign of large-scale magnetic topology. The coronal variations are roughly synchronous with those observed in the chromosphere, and we find that the minimum X-ray activity corresponds to phases with a magnetic flux maximum in the radial field component. This follows expectations, since radial magnetic fields are associated with open coronal structures that are usually X-ray faint.

Based on our spectral analysis of τ Boo, we derive X-ray luminosities in the range of $5\text{--}8 \times 10^{28}$ erg s $^{-1}$, including about 1×10^{28} erg s $^{-1}$ from the secondary. This makes τ Boo A a moderately active star with a mean $\log L_X/L_{\text{bol}} = -5.3$. The spectra of the individual exposures are quite similar, and when folding the X-ray luminosities with the cycle period used above, the long-term X-ray luminosity variations are again remarkably well described by a 120-day period, as shown in Fig. 7. The amplitude of the X-ray cycle as seen in the *XMM-Newton* data is modest, with $L_{X,\text{max}}/L_{X,\text{min}} \approx 1.6$. Given these results, it is not surprising or contradicting that Poppenhaeger et al. (2012) failed to detect a one-year cycle in their analysis of six datasets.

The coronal temperatures are quite stable over the cycle, with dominant plasma components being present at 2.5–3.0 MK and around 6 MK. At activity minimum, the cooler plasma is slightly more pronounced. Emission measure ratios are found to be in the range $EM_{\text{cool}}/EM_{\text{hot}} \approx 2.0\text{--}1.2$ for our data. The activity cycle is driven by variations of the emission measure, and summed values are around $EM = 3.5 (\pm 1) \times 10^{51}$ cm $^{-3}$ for solar or mildly sub-solar abundances. The X-ray derived values are roughly an order of magnitude above the estimates by Vidotto et al. (2012), where the EM was computed in the closed field line regions of magnetic field configurations derived from surface magnetic maps. Since the X-ray emitting plasma is largely connected to coronal loop structures, the difference is significant. Moreover, plasma not contributing to the observed X-ray emission would add to the discrepancy. This indicates that a large part of the presumably small-scale magnetic structure is not covered by the constructed surface maps and derived field configurations. However, the temporal evolution of the reconstructed large-scale

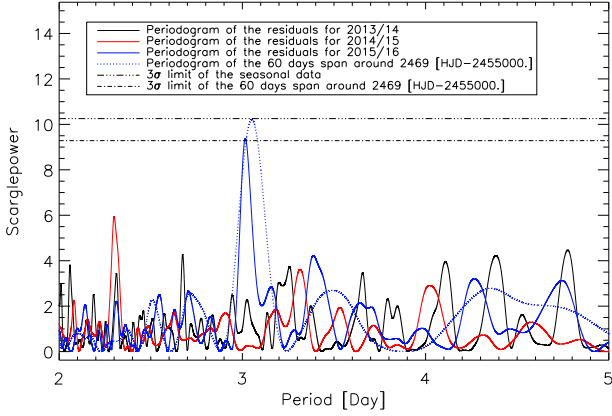


Fig. 8. Periodogram of the residuals of the sinusoidal fit with the 60-day period for the third observation season.

magnetic field, based on the same spectropolarimetric observations (Fares et al. 2013), agrees well with those seen in the X-ray data. A comparison of our results with X-ray data taken over the past decades yields overall consistent values, indicating a long-term stability of the global coronal properties of τ Boo.

3.4. *S*-index: rotational period

The sampling of our τ Boo *S*-index time series also allows us to check whether the *S*-index data are modulated with the expected rotational period of about three days. For this exercise we use the residuals of the sinusoidal fits with the periods listed in Table 5 that describe the long-term behavior of our LS analysis. At this point, we would like to emphasize again the importance of detrending, since an unconsidered long-term trend or a longer period would change the power in the periodogram. The rotational variation could be weak compared to a long-term trend or the variation by a possible activity cycle.

In the data of the first two seasons we do not find any evidence of the rotational period in the LS periodograms (see Fig. 8). In the data of the season 2015–16, however, we find a periodic signal in the residuals at a period of 3.02 ± 0.01 days with a significance of 99.12% (see Fig. 8). The corresponding window function is shown in the Fig. 9. This period is also visible in the periodogram for the *S*-index time series for the season 2015–16, where the ≈ 60 -day period is not removed. Here, the significance of this period is 98.4%.

Additionally, we tested whether the period and significance of the rotational period signal change with time. To do so, the time series was split into 60-day chunks that were then shifted by 10 days, except for the data before 2419 [HJD-2 455 000] because there the data sampling is not suitable to find a 3-day period. We find that the periods determined in this way are consistent with the 3.02-day period found in the total time series. However, the significance of the rotational period changes with time; the results are listed in Table 6. We find the strongest signal for the time around 2469 [HJD-2 455 000] with a significance of 99.89% and a period of 3.05 ± 0.01 days, see Fig. 8. The corresponding window function is shown in Fig. 9.

This period has the highest significance, therefore we take this period as the rotational period of τ Boo for this observation season.

Our period of 3.05 days is consistent with the period of 3.3 ± 0.5 days by Baliunas et al. (1997) and is located the period range from ≈ 2.6 to 4.1 days obtained by Henry et al. (2000).

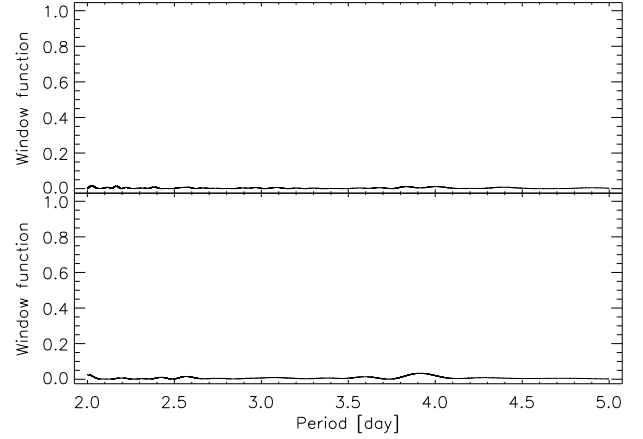


Fig. 9. Window functions for rotational period estimation. The *upper plot* shows the window function for the entire seasonal data 2015–16. The *lower plot* shows the window function for the seasonal data 2015–16 of the 60-day chunk with the highest peak.

Table 6. Mean time of the time interval, number of S_{MWO} , rotational period, FAP, and significance.

HJD – 2 455 000 [Day]	Mean time	No. of S_{MWO}	Period [Day]	FAP	Sig. [%]
2449		45	3.05 ± 0.02	8.96×10^{-2}	91.04
2459		49	3.04 ± 0.02	9.23×10^{-3}	99.08
2469		47	3.05 ± 0.01	1.10×10^{-3}	99.89
2479		48	3.09 ± 0.02	3.63×10^{-3}	99.64
2489		52	3.02 ± 0.02	3.04×10^{-2}	96.96

The slight differences to the period by Baliunas et al. (1997) and also the period range reported by Henry et al. (2000) might be explained by differential rotation, which has been recognized in τ Boo by Reiners (2006) or Borsa et al. (2015).

In order to assess the influence of the ≈ 60 -day period and the jump on the rotation period analysis, the analysis was repeated without removing the ≈ 60 -day period. We find – within the margins of uncertainty – the same periods, but with lower significance. This shows that the ≈ 60 -day period and the jump only influence the significance of the found periods, but not the periods themselves.

4. Discussion and conclusion

Our TIGRE *S*-index time series covers an overall time span of around three years and contains at least one activity cycle in each observation season. The derived mean cycle period of 122 days is consistent with previous results and suggests that the periodicity is a persistent feature of the magnetic activity of τ Boo, which appears to have been present at least during about the past fifty years. The available X-ray data – taken with *XMM-Newton* and rereduced – also support a cyclic behavior when phase-folded with the same period, suggesting that the chromospheric and coronal properties of τ Boo change in parallel, as observed for the Sun and stars like 61 Cyg A (Robrade et al. 2012). Recently, Boro Saikia et al. (2016) reported an analysis of ZDI maps with a detection of a magnetic cycle on 61 Cyg A, in phase with the well-known chromospheric and coronal activity cycle. The finding of connected cycles in stars over a broad range, for example, F type (τ Boo), G type (Sun), and K type (61 Cyg A), suggests

that this might be a general characteristic of activity cycles of cool main-sequence stars.

The X-ray brightness variations in the corona of τ Boo over its cycle are with a factor of less than two smaller than those observed in stars of later spectral type with moderate activity level. Although the number of studied objects is small, these stars typically have cycles with larger relative X-ray flux variations and longer periods (Robrade et al. 2012). Overall, the coronal properties of τ Boo are more similar to those of the F8 star ι Hor (Sanz-Forcada et al. 2013), which exhibits a 1.6 yr magnetic activity cycle with some temporal irregularities. These similarities might point at shorter and less pronounced coronal cycles in F stars with their higher luminosities and shallower convection zones.

Furthermore, τ Boo did exhibit an unusual activity behavior in the observation season 2015–16, when the S -index suddenly jumped from the assumed maximum to a minimum and then again started to increase. It is unknown how frequently such events occur. Furthermore, in our TIGRE S -index time series we find evidence of a period of 3.05 days, the presumed rotation period, only in the third observation season, while no significant power is seen around this period during the first two seasons. The derived period of 3.05 days is consistent with the rotation period reported by Baliunas et al. (1997) and with the findings of Henry et al. (2000), who reported periods in the range from ≈ 2.6 to 4.1 days, where our signal is also located. The MOST data presented by Walker et al. (2008) also agree with our results. Furthermore, the period we found is consistent with the average period determined from Donati et al. (2008), Fares et al. (2009, 2013) and Mengel et al. (2016) of ≈ 3.1 days. We therefore feel confident in identifying our 3.05-day period with the rotation period of τ Boo. Furthermore, the differential rotation of τ Boo must be kept in mind, since differential rotation can lead to different periods in different observational seasons, depending on the dominating spot latitudes.

Fares et al. (2009) reported the discovery of two magnetic polarity changes detected in τ Boo with the help of ZDI. Specifically, Fares et al. (2009) presented four ZDI images of τ Boo, taken in July 2007, January 2008, June 2008, and July 2008. The authors argued that a polarity switch took place between January and June 2008. Since another switch had been observed earlier between July 2006 and July 2007 (cf. Donati et al. 2008), these authors argued that the magnetic cycle period of τ Boo ought to be 2 yr as opposed to the 22-yr magnetic cycle period of the Sun. Fares et al. (2013) also estimated a 2-yr magnetic cycle, but did not rule out an 8-month magnetic cycle, which would correspond to a 4-month activity cycle. Further ZDI maps of τ Boo were presented by Fares et al. (2009, 2013) and by Mengel et al. (2016), and so far, a total of 14 ZDI maps of τ Boo have been constructed. Specifically, Mengel et al. (2016) presented ZDI maps of τ Boo that were constructed with data taken in the periods 4.12.13–21.12.13, 4.5.14–18.5.14, 6.1.15–18.1.15 14, and 12.3.15–27.5.15, that is, at times, when (pseudo-)simultaneous TIGRE coverage was also available.

In the Sun the magnetic polarity reversals occur near solar maximum, hence we may speculate that the cyclic Ca II H and K variations observed by TIGRE are accompanied by magnetic polarity switches as reported by Donati et al. (2008), Fares et al. (2009), Fares et al. (2013), and Mengel et al. (2016). Such polarity switches would then occur – approximately – every four months. Mengel et al. (2016) reported polarity reversals between December 2013 and May 2014 and between January and March 2015. Our S -index light curves peak at 2014 March 1 and 2015 March 1. The hypothesis of a solar-like behavior, that

is, polarity reversal at maximum, is therefore entirely consistent with the ZDI data.

In a study of the character of chromospheric activity as a function of stellar mass and relative MS age in the sample of stars studied by Baliunas et al. (1995; Schröder et al. 2013), we found that solar-type activity cycles of about 10 yr duration only occur for about one solar mass and below, and they seem to be absent on the MS for the more massive F stars. Instead, F stars of solar activity level were classified as irregular or long-term variable, but a relatively low cadence of their monitoring could easily overlook a period as short as a few months, even though the case of τ Boo was correctly recognized. This raises two interesting questions for future research: (i) Is τ Boo with its fast activity period representative for F stars on the MS? And (ii), if so, does this much shorter period indicate a change to a different dynamo type, perhaps related to the geometrically thinner convective envelopes of F stars? These questions can only be resolved with monitoring more F stars and their activity. In this context, the *Kepler* data could be interesting to investigate F-type stars, regardless of whether a magnetic cycle is visible (Mathur et al. 2014). Mathur et al. (2014) observed 22 F-type stars with *Kepler* and investigated them to find evidence of magnetic activity or a magnetic cycle. The authors found two stars with evidence of a magnetic cycle.

In summary, the activity behavior of τ Boo therefore appears to be very similar to that of the Sun in terms of correlated chromospheric and coronal properties and magnetic polarity reversals at cycle maximum, but the cycle timescale is more than 30 times faster than for the Sun. The magnetic field measurements and the ZDI images provide a good visualization of the magnetic field configuration and constitute an excellent method to monitor the activity cycle of τ Boo in connection with longer term chromospheric and coronal monitoring. We caution, however, that phase jump events such as observed in the season 2015–16 might change the situation altogether. An analysis of historic Mount Wilson data might provide clues as to the frequency of such events. More multiwavelength observations of τ Boo are clearly required to better understand the complex pattern of its magnetic activity.

Acknowledgements. This work is based on observations obtained with *XMM-Newton*, an ESA science mission with instruments and contributions directly funded by ESA Member States and NASA. J.R. acknowledges support from the DLR under grant 50QR0803. We acknowledge the continued support by various partners who helped to realize TIGRE. In the first place, this is the University of Hamburg, which gave support in terms of funding, manpower, and workshop resources. Furthermore, grants from the Deutsche Forschungsgemeinschaft (DFG) in various funding lines are gratefully acknowledged, as well as travel money from both the DFG and DAAD, and from CONACyT in several bilateral grants. The Liège contribution to TIGRE is funded through an opportunity grant from the University of Liège. The Universities of Guanajuato and Liège and the Mexican state of Guanajuato shared the funding of the infrastructure required by TIGRE at the La Luz site, and there is continued support by the University of Guanajuato in terms of manpower and running costs of the facilities.

References

- Baliunas, S. L., Donahue, R. A., Soon, W. H., et al. 1995, *ApJ*, 438, 269
- Baliunas, S. L., Henry, G. W., Donahue, R. A., Fekel, F. C., & Soon, W. H. 1997, *ApJ*, 474, L119
- Boro Saikia, S., Jeffers, S. V., Morin, J., et al. 2016, *A&A*, 594, A29
- Borsa, F., Scandariato, G., Rainer, M., et al. 2015, *A&A*, 578, A64
- Butler, R. P., Marcy, G. W., Williams, E., Hauser, H., & Shirts, P. 1997, *ApJ*, 474, L115
- Catala, C., Donati, J.-F., Shkolnik, E., Bohlender, D., & Alecian, E. 2007, *MNRAS*, 374, L42
- Collier Cameron, A., & Leigh, C. 2004, *Astron. Nachr.*, 325, 252
- Cumming, A., Marcy, G. W., & Butler, R. P. 1999, *ApJ*, 526, 890

- de la Calle, I. 2014, <http://www.cosmos.esa.int/web/xmm-newton>
- Donati, J.-F., Moutou, C., Fares, R., et al. 2008, *MNRAS*, **385**, 1179
- Eberhard, G., & Schwarzschild, K. 1913, *ApJ*, **38**, 292
- Fares, R., Donati, J.-F., Moutou, C., et al. 2009, *MNRAS*, **398**, 1383
- Fares, R., Moutou, C., Donati, J.-F., et al. 2013, *MNRAS*, **435**, 1451
- García, R. A., Mathur, S., Salabert, D., et al. 2010, *Science*, **329**, 1032
- Hall, J. C., Lockwood, G. W., & Skiff, B. A. 2007, *AJ*, **133**, 862
- Hempelmann, A., Mittag, M., Gonzalez-Perez, J. N., et al. 2016, *A&A*, **586**, A14
- Henry, G. W., Baliunas, S. L., Donahue, R. A., Fekel, F. C., & Soon, W. 2000, *ApJ*, **531**, 415
- Horne, J. H., & Baliunas, S. L. 1986, *ApJ*, **302**, 757
- Hünsch, M., Schmitt, J. H. M. M., & Voges, W. 1998, *A&AS*, **132**, 155
- Isaacson, H., & Fischer, D. 2010, *ApJ*, **725**, 875
- Leigh, C., Collier Cameron, A., Horne, K., Penny, A., & James, D. 2003, *MNRAS*, **344**, 1271
- Maggio, A., Sanz-Forcada, J., & Scelsi, L. 2011, *A&A*, **527**, A144
- Mathur, S., García, R. A., Ballot, J., et al. 2014, *A&A*, **562**, A124
- Mengel, M. W., Fares, R., Marsden, S. C., et al. 2016, *MNRAS*, **459**, 4325
- Metcalfe, T. S., Basu, S., Henry, T. J., et al. 2010, *ApJ*, **723**, L213
- Mittag, M., Schröder, K.-P., Hempelmann, A., González-Pérez, J. N., & Schmitt, J. H. M. M. 2016, *A&A*, **591**, A89
- Oláh, K., Kővári, Z., Petrovay, K., et al. 2016, *A&A*, **590**, A133
- Piskunov, N. E., & Valenti, J. A. 2002, *A&A*, **385**, 1095
- Poppenhaeger, K., Günther, H. M., & Schmitt, J. H. M. M. 2012, *Astron. Nachr.*, **333**, 26
- Poppenhaeger, K., & Wolk, S. J. 2014, *A&A*, **565**, L1
- Reiners, A. 2006, *A&A*, **446**, 267
- Robrade, J., Schmitt, J. H. M. M., & Favata, F. 2012, *A&A*, **543**, A84
- Sanz-Forcada, J., Stelzer, B., & Metcalfe, T. S. 2013, *A&A*, **553**, L6
- Schmitt, J. H. M. M., Golub, L., Harnden, Jr., F. R., et al. 1985, *ApJ*, **290**, 307
- Schmitt, J. H. M. M., Schröder, K.-P., Rauw, G., et al. 2014, *Astron. Nachr.*, **335**, 787
- Schröder, K.-P., Mittag, M., Hempelmann, A., González-Pérez, J. N., & Schmitt, J. H. M. M. 2013, *A&A*, **554**, A50
- Shkolnik, E., Walker, G. A. H., Bohlender, D. A., Gu, P.-G., & Kürster, M. 2005, *ApJ*, **622**, 1075
- Smith, R. K., Brickhouse, N. S., Liedahl, D. A., & Raymond, J. C. 2001, *ApJ*, **556**, L91
- Vidotto, A. A., Fares, R., Jardine, M., et al. 2012, *MNRAS*, **423**, 3285
- Walker, G. A. H., Croll, B., Matthews, J. M., et al. 2008, *A&A*, **482**, 691
- Wilson, O. C. 1978, *ApJ*, **226**, 379
- Zechmeister, M., & Kürster, M. 2009, *A&A*, **496**, 577